Multilayer black phosphorus as saturable absorber for an $Er:Lu_2O_3$ laser at ~3 μm

Mingqi Fan,[1] Tao Li,[1,*] Shengzhi Zhao,[1] Guiqiu Li,[1] Xiaochun Gao,[2] Kejian Yang,[1] Dechun Li,[1] and Christian Kränkel[3,4,5]

[1]*School of Information Science and Engineering, and Shandong Provincial Key Laboratory of Laser Technology and Application, Shandong University, Jinan 250100, China*
[2]*Key Laboratory of Colloid and Interface Chemistry of State Education Ministry, School of Chemistry and Chemical Engineering, Shandong University, Jinan 250100, China*
[3]*Institut für Laser-Physik, Universität Hamburg, Luruper Chaussee 149, 22761 Hamburg, Germany*
[4]*Hamburg Centre for Ultrafast Imaging, Universität Hamburg, Luruper Chaussee 149, 22761 Hamburg, Germany*
[5]*e-mail: kraenkel@physnet.uni-hamburg.de*
**Corresponding author: litao@sdu.edu.cn*

Received June 24, 2016; revised July 20, 2016; accepted July 20, 2016;
posted July 22, 2016 (Doc. ID 269206); published September 6, 2016

Multilayer black phosphorus (BP) nanoplatelets of different thicknesses were prepared by the liquid phase exfoliation method and deposited onto yttrium aluminum garnet substrates to form saturable absorbers (SAs). These were characterized with respect to their thickness-dependent saturable absorption properties at 3 μm. The BP-SAs were employed in a passively *Q*-switched $Er:Lu_2O_3$ laser at 2.84 μm. By using BP exfoliated in different solvents, stable pulses as short as 359 ns were generated at an average output power of up to 755 mW. The repetition rate in the experiment was 107 kHz, corresponding to a pulse energy of 7.1 μJ. These results prove that BP-SAs have a great potential for optical modulation in the mid-infrared range.

OCIS codes: (160.3380) Laser materials; (140.3070) Infrared and far-infrared lasers; (140.3540) Lasers, Q-switched.
http://dx.doi.org/10.1364/PRJ.4.000181

1. INTRODUCTION

The research in newly emerging saturable absorber (SA) materials primarily focuses on graphene and graphene-like two-dimensional (2D) materials [1–4]. Compared with conventional SAs, such as semiconductor SA mirrors and ion-doped crystals [5,6], these new nanomaterials are favorable for many applications due to their fascinating advantages of broadband saturable modulation, controllable modulation depth, and ultrafast recovery time [7]. However, there is still a bottleneck in the field of modulated mid-infrared (mid-IR) lasers based on 2D-SAs. Graphene suffers from the intrinsic limitation of its zero-bandgap structure, which increases the nonsaturable optical absorption (~2.3% per layer) [8]. For other effective 2D-SAs such as topological insulators like Bi_2Te_3, Bi_2Se_3, and Sb_2Te_3 [9], the complex preparation process severely limits their application in photonics and optoelectronics. Finally, in semiconducting transition metal dichalcogenides, such as molybdenum disulfide (MoS_2), the optical response is mainly confined to the visible and near-IR range, due to their comparatively large bandgap (MoS_2-monolayer: direct bandgap of 1.86 eV; MoS_2-bulk: indirect gap of 0.86–1.29 eV) [10].

Black phosphorus (BP), a novel class of 2D materials, has a direct bandgap, which depends on the number of layers and decreases with increasing thickness, ranging from ~2.0 eV (monolayer) to ~0.3 eV (bulk) [11]. This unique feature makes it a promising candidate for photonics applications in a broad wavelength range between 0.6 and 4.1 μm. So far, BP-SAs have been widely employed as modulators in passively *Q*-switched or mode-locked lasers at 1 and 2 μm [12–15]. At 3 μm only one report by Kong *et al.* can be found, who realized a pulsed bulk laser with a very long pulse duration of 4.5 μs [16]. Except for this, only a few relevant studies on BP modulated fiber lasers in this wavelength range have been reported [17,18].

In 1967, Robinson and Devor demonstrated the first Er^{3+}-doped laser at 3 μm on the $^4I_{11/2} \rightarrow {}^4I_{13/2}$ transition [19]. However, it proved difficult to optimize the performance of Er^{3+}-doped 3-μm lasers due to the severe thermal effects, which are induced by the low Stokes efficiency (~35%) and the strong multiphonon relaxation. The cubic rare-earth sesquioxide crystals, with high thermal conductivity and low phonon energies [20,21], have been proven to be suitable host materials for mid-IR lasers. In previous works, up to 14 W of laser output around 3 μm have been generated with $Er:Y_2O_3$ at cryogenic temperatures [22], and at room temperature 5.9 W of continuous wave (CW) laser output were realized with $Er:Lu_2O_3$ [23]. Recently, we demonstrated an efficient passively *Q*-switched $Er:Lu_2O_3$ laser using stoichiometric-defect MoS_2-SA, which generated the shortest pulses of any 2D-SA *Q*-switched 3 μm laser with more than 1 W of average output power [24].

Pulsed lasers around 3 μm, which is well within the eye-safe region and can be strongly absorbed by water, are sought after in biomedical applications [25]. Besides, such lasers also have particularly practical value in mid-IR optical parametric oscillators and generation of terahertz (THz) and IR supercontinuum light [26,27].

In this contribution, we prepared multilayer BP nanoplatelets based on the liquid phase exfoliation (LPEx) method and

deposited them on yttrium aluminum garnet (YAG) substrates to fabricate a novel BP-SA for the mid-IR. A series of measurements was conducted to characterize the layer-dependent saturable absorption properties of the BP-SA samples near 3 μm. Finally, a stable passively *Q*-switched laser operating at 2.84 μm was realized, delivering a maximum average power of 755 mW with a pulse duration of 359 ns and a pulse energy of up to 7.1 μJ.

2. PREPARATION AND CHARACTERIZATION OF BP-SAS

BP is a room-temperature stable orthorhombic modification of phosphorus, which exhibits a graphite-like layer structure [28] and gives rise to saturable absorption properties which strongly depend on the number of layers. LPEx is an effective method for the fabrication of such multilayer structures, in which the choice of a proper solvent plays a key role. In order to prepare high quality BP nanoflakes of different thicknesses, both pure isopropyl alcohol (IPA) and saturated NaOH N-methyl-2-pyrrolidone (NMP) solvent were used in our experiment [12,29]. In both cases, exfoliation could be obtained by adding bulk BP into the selected solvent and ultrasonicating for 6 h. After centrifugation at 1500 rpm for 10 min, the top two-thirds of the dispersions were collected for further processing. Since NMP has a poor volatility, the multilayer BP nanoplatelets exfoliated by saturated NaOH NMP solvent were additionally separated and rediluted in ethanol (EtOH) solution to remove the remaining Na^{3+}-ions.

For a systematic characterization of the structure and morphology of the BP samples, transmission electron microscopy (TEM) and Raman spectroscopy were utilized. As shown in Figs. 1(a) and 1(b), the TEM pictures clearly prove that the as-prepared BP nanoplatelets have sheet-like structures with submicrometer dimensions. The Raman spectra shown in Fig. 1(c) were measured by using a HeNe laser at 632.8 nm. One out-of-plane vibration mode (A_g^1) and two in-plane vibration modes (B_{2g} and A_g^2) were detected. Compared to the BP-bulk curve, all three peaks in BP-IPA and BP-EtOH curves exhibit a blueshift. The A_g^2 vibration mode is more sensitive to the number of layers; therefore the distance between A_g^1 and A_g^2 modes changes for samples of different thickness. These Raman shifts indicate a decreased

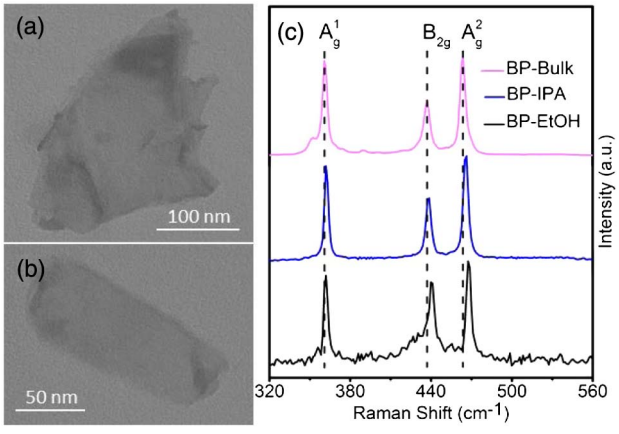

Fig. 1. TEM images of BP nanoplatelets exfoliated in (a) IPA (BP-IPA) and (b) EtOH solution (BP-EtOH), (c) Raman spectra of the nanoplatelets in comparison to bulk BP.

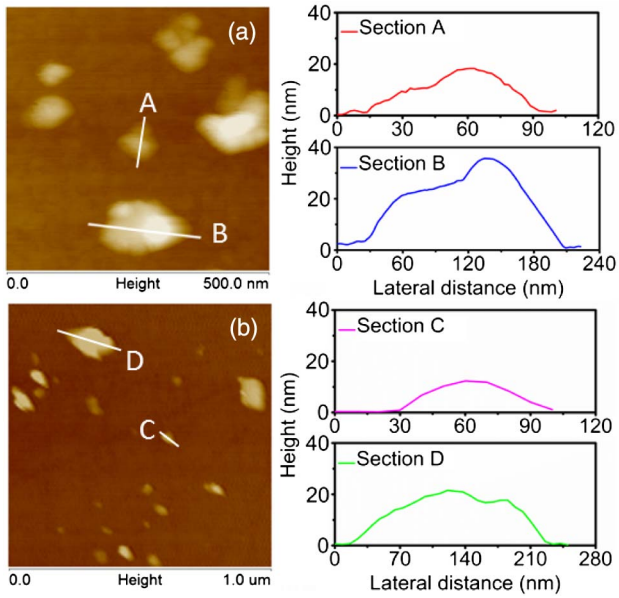

Fig. 2. AFM images and typical height profiles: (a) BP-IPA and (b) BP-EtOH samples.

thickness compared to the bulk material and thus the successful exfoliation of BP samples [29,30]. Furthermore, the characteristic peaks of the BP-EtOH curve at 362.1, 439.8, and 467.4 cm^{-1} show a stronger blueshift than the BP-IPA peaks at 361.9, 438.7, and 466.2 cm^{-1}, which is a first indicator for a lower number of layers in the samples prepared in BP-EtOH.

Atomic force microscopy (AFM) was used to precisely analyze the thickness of the BP dispersed in the different solvents [see Figs. 2(a) and 2(b)]. Assuming a single layer thickness of ~0.6 nm of BP [31], the number of layers of the BP nanoplatelets exfoliated in IPA was calculated to be between 28 and 52, whereas the platelets dissolved in EtOH exhibit a thickness of only 19–35 layers. The lower thickness of the BP-EtOH compared to the BP-IPA is in good agreement with the results of TEM and Raman measurements.

Fourier transform IR (FT-IR) absorption spectra were recorded to analyze the broadband absorption capability of the BP. As shown in Fig. 3(a), the BP-EtOH film coating on a YAG substrate with dimensions of 40 mm × 20 mm exhibits a gradually decreasing absorption in the whole wavelength range from 0.8 to 3.3 μm.

BP-SAs were fabricated by dripping the BP dispersions onto round YAG substrates with a radius of 0.5 in. (1.27 cm) and drying in a vacuum oven at room temperature for 10 h. Unlike the samples used in TEM and AFM, for which a tiny amount of dispersion is preferred in that BP nanoplatelets could be clearly observed and measured, the dosage for BP-SAs could only be optimized according to the results of the laser experiment.

We performed small-signal transmission measurements for the BP-SAs used in the laser experiments. For this purpose we used a CW Er:Lu_2O_3 laser [24]. The resulting values for the BP-IPA-SA and the BP EtOH-SA were 78% and 82.6%, respectively. The mismatch of the unsaturated absorption compared to the FT-IR measurement shown in Fig. 3(a) results from a different BP-nanoplatelet density on the two different substrates used for the respective experiments. Besides, the FT-IR spectra were corrected for Fresnel reflection, which was not possible

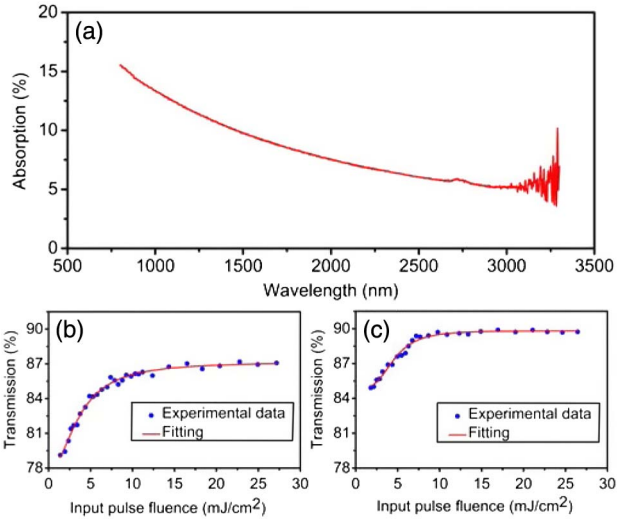

Fig. 3. (a) FT-IR absorption spectrum of a BP-EtOH test sample on a 40 mm × 20 mm YAG plate; (b) and (c) depict the nonlinear transmission of BP-IPA and BP-EtOH SAs.

for the CW Er:Lu_2O_3 due to Fabry–Perot effects in the plane-parallel YAG substrates of the SAs. The nonlinear optical response of the BP-SAs was investigated using a ~100 ns *Q*-switched Er:Lu_2O_3 laser at 2.84 μm as shown in Figs. 3(b) and 3(c) [24]. One can recognize a significant difference in the saturable absorption between the samples prepared in IPA and EtOH, which we attribute to the different thickness of the BP nanoplatelets. The modulation depths of the BP-IPA-SA and the BP-EtOH-SA were estimated to be 8.0% and 5.0%, respectively. This is in line with the different thicknesses of the BP nanoplatelets prepared in both solvents. Considering the ultrafast recovery time of 24 ± 2 fs in BP [32], there was less meaning in assessing the saturation fluence with a submicrosecond pulsed source. The saturated transmission of the BP-IPA-SA and the BP-EtOH-SA amounted to 87.1% and 89.8%, respectively; however, the uncoated YAG substrates exhibit a transmission of only 93.2% due to surface reflection, which, however, does not represent losses when inserted perfectly perpendicular to the beam into a laser cavity. Accordingly, the nonsaturable loss of BP-IPA and BP-EtOH films were estimated to be 6.1% and 3.4%, respectively. The lower nonsaturable losses of the BP-EtOH-SA compared with BP-IPA-SA can be attributed to the decrease of the BP concentration induced by the redilution process.

These results are well suited for the application of these samples as SAs in our Er:Lu_2O_3 laser and prove that BP layers of different thickness have a great potential to cover a large parameter room, which makes them suitable also for other laser systems in this wavelength range.

3. LASER EXPERIMENT

A. Experimental Setup

The Er:Lu_2O_3 crystal prepared for our experiment had an Er^{3+} concentration of 7 at. % and dimensions of 3 mm × 3 mm × 8 mm. It has already been proved to be an excellently suited gain medium for efficient high-power lasing at 3 μm [23,24]. The Er:Lu_2O_3 crystal was wrapped in indium foil and embedded in a cooper block water-cooled to 10°C. The cavity for the laser experiments on passive *Q*-switching using

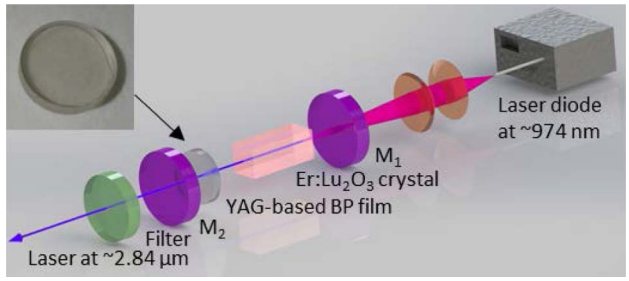

Fig. 4. Schematic diagram of the *Q*-switched Er:Lu_2O_3 laser and the BP-IPA SA (inset).

our BP-SAs was a simple, 2.5-cm-long compact linear cavity, as schematically presented in Fig. 4. A fiber-coupled laser diode with 200 μm core diameter and a numerical aperture of 0.22 was taken as the pump source. The emission wavelength could be adjusted by changing the diode temperature to match the absorption peak of Er:Lu_2O_3 at 974 nm, while preventing wavelengths of strong exited-state absorption [23]. The pump beam was focused into the gain medium with a spot diameter of 400 μm. The flat incoupling mirror M_1 was antireflection coated for 974 nm (T > 90%) and high-reflection coated for the laser wavelength range between 2.7 and 2.9 μm (R > 99%). Flat mirrors with transmission values of 1%, 3%, and 5% at 2.85 μm were employed as the output coupling mirror M_2. The BP-SA-films on YAG substrates were placed in the beam near M_2. The mode radius on the SA was estimated to be ~300 μm. In order to block the residual pump light, a filter was put behind M_2. The average output power was measured by a PM100D power meter with an S314C power head (Thorlabs Inc., USA). The emission spectrum was detected by an InSb infrared detector (DInSb5-De01, Zolix, China) and analyzed with a grating spectrometer (Omni-λ300, Zolix, China). The temporal evolution of the laser pulse trains was monitored by a DPO 7104C digital phosphor oscilloscope with a rise time of 350 ps (1 GHz bandwidth and 20 GS/s sampling rate, Tektronix Inc., USA), combined with a fast HgCdTe IR detector with a response time of 20 ns (PVI-2TE-5, Vigo System S.A.)

B. Results and Discussion

Stable *Q*-switched laser operation could be achieved with either BP-SA in the cavity. Figure 5 shows the *Q*-switched laser characteristics for both cases. Employing the BP-IPA sample, the threshold pump powers were 1.09, 1.41, and 1.91 W at T = 1%, 3%, and 5%, respectively. Increasing the absorbed pump power to 5.91 W, the highest average output power of 755 mW was obtained at T = 3% with a slope efficiency of 17.9%. By optimizing the technology of mirror-coating and cooling the crystal and SA with nitrogen, the investigation realizing higher slope efficiency can be expected. In addition, at even higher pump power levels, the *Q*-switched pulse train became unstable and finally went into CW mode. By reducing the pump power, the laser switched back into *Q*-switched operation. This phenomenon, known as overbleaching of the SA [33], occurred as the CW intracavity power was high enough to saturate the absorber. For this reason, the significant increase in maximum output power becomes particularly difficult. The BP-EtOH *Q*-switched laser exhibits a slightly lower threshold and a marginally higher

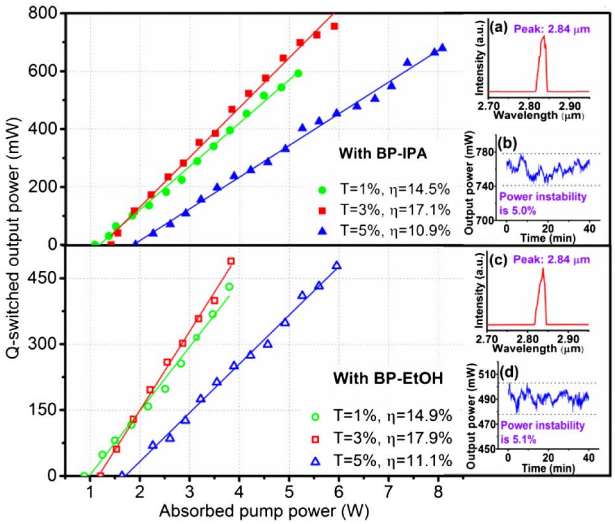

Fig. 5. Average output power of the Q-switched Er:Lu_2O_3 laser using BP-SA; insets (a) and (c) display the output laser spectra, and insets (b) and (d) describe the output fluctuations versus time.

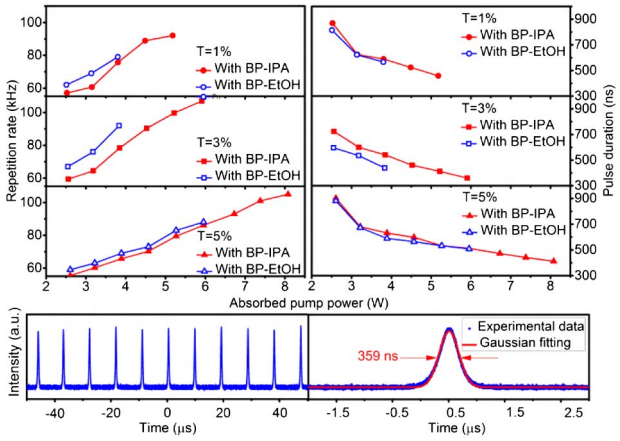

Fig. 6. Top: pulse repetition rate and pulse duration versus absorbed pump power for different output coupler transmissions, bottom: temporal traces of Q-switched pulse train utilizing BP-IPA SA at T = 3%.

slope efficiency compared to the BP-IPA Q-switched laser. However, Q-switching with the BP-EtOH film was stable only up to 3.84 W of absorbed pump power at T = 3%. This earlier onset of bleaching by the CW intracavity power is in good agreement with the results of the nonlinear optical response measurements, which revealed a lower saturation intensity for the BP-EtOH S.A.

The laser emission spectra are presented in the insets (a) and (c) of Fig. 5. The center wavelengths of both lasers were fixed to 2.84 μm. Besides, the fluctuations of the two lasers were detected for 40 min at the maximum output power, as shown in the insets (b) and (d) of Fig. 5. The stability of both lasers was quite comparable to the results presented in [24], where MoS_2 was used as the SA. This indicates that the instability is not attributed to the properties of the BP-SAs but is intrinsic to the complex transition processes in the Er^{3+} ion.

Figure 6 depicts the pulse characteristics versus pump power and output coupler transmission in detail. The pulse repetition rate increases with absorbed pump power, while the pulse duration exhibits an opposite trend. At identical pump power levels, the BP-EtOH-based film generated shorter pulses of 439 ns at a higher repetition rate of 92 kHz. However, the shortest pulse duration of 359 ns at a repetition rate of 107 kHz was obtained by using the BP-IPA-SA under an absorbed pump power of 5.91 W at T = 3%. The pulse train and the temporal profile of a single pulse are shown as an example in the lower part of Fig. 6. The pulse-to-pulse instability was found to be below 10%, which indicates that the BP-IPA film is still working quite stably at an average power as high as 755 mW.

Table 1 summarizes the results obtained with other 2D-SA Q-switched lasers in the 3-μm wavelength range compared to our result. It should be noticed that, excepting the SAs, the pulse duration was also strongly influenced by cavity design and laser parameters. The pulse durations generated in this work are much shorter than those obtained by graphene and Bi_2Te_3 SAs, and are comparable to the results generated by MoS_2 SAs. The compact cavity design in this work made a contribution to compressing the pulses. This comparison also illustrates that the YAG-based BP-IPA film is suitable for Q-switched solid-state 3 μm lasers, while the BP-EtOH film or the thinner BP nanoflakes might even enable mode-locking of Er^{3+}-doped laser at 3 μm. Experiments in this respect are in progress.

Figure 7 depicts the pulse energies and peak powers, which both increased with the absorbed pump power. The Er:Lu_2O_3 crystal had absorbed about 90% pump power, and the two samples worked well during the laser experiments, even under the available high power levels. At T = 3%, the maximum single pulse energies were 7.1 and 5.3 μJ, respectively. Assuming a Gaussian pulse shape, which is justified by the measured pulse shape shown in Fig. 6, the highest peak power of 18.6 W was obtained at T = 3% with the BP-IPA-SA.

4. CONCLUSION

In conclusion, multilayer BP nanoplatelets were prepared based on the LPEx method, and BP-SAs were fabricated by spreading the dispersions over YAG substrates. The layer-dependent saturable absorption properties near 3 μm were experimentally demonstrated. Stable BP-IPA and BP-EtOH

Table 1. Comparison of 3 μm Lasers Q-Switched with 2D-SAs

Type of SA	Graphene	Bi_2Te_3	BP-SAM	BP Gold-Film Mirror	MoS_2	BP-IPA	BP-EtOH
Gain medium	Er^{3+}-fiber	Ho^{3+}-fiber	Er^{3+}-fiber	Er:Y_2O_3 ceramic	Er:Lu_2O_3 crystal	Er:Lu_2O_3 crystal	Er:Lu_2O_3 crystal
Wavelength (μm)	2.78	2.98	2.78	2.72	2.84	2.84	2.84
Max. output power (mW)	62	327.4	485	6	1030	755	489
Max. repetition rate (kHz)	37	82	63	12.6	121	107	92
Shortest pulse duration (μs)	2.9	1.37	1.18	4.47	0.335	0.359	0.439
Reference	[34]	[35]	[16]	[18]	[24]	This work	This work

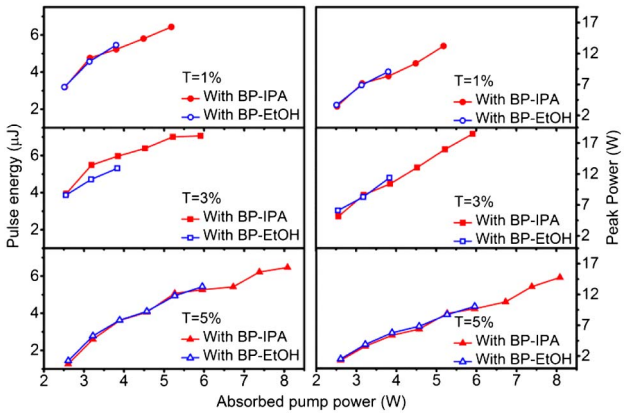

Fig. 7. Evolutions of the single pulse energy and peak power as increasing absorbed pump power for different output coupler transmissions.

passively *Q*-switched Er:Lu_2O_3 laser operation at 2.84 μm was realized. The minimum pulse duration of 359 ns was obtained at the highest average output power of 755 mW, corresponding to a pulse energy of 7.1 μJ. The results validate that BP is a promising optical modulator for mid-IR pulse lasers and has great potential in ultrafast photonics applications.

Funding. China Postdoctoral Science Foundation (2014M561921, 2015T80713); Independent Innovation Foundation of Shandong University (IIFSU) (2082014TB011); Innovation Foundation of the 46th Institute of China Electronics Technology Group Corporation (CJ20130302); National Natural Science Foundation of China (NSFC)) (61308020); Deutsche Forschungsgemeinschaft (DFG) (FKZ 13N13050).

REFERENCES

1. F. Bonaccorso, Z. Sun, T. Hasan, and A. C. Ferrari, "Graphene photonics and optoelectronics," Nat. Photonics **4**, 611–622 (2010).
2. X. L. Qi and S. C. Zhang, "Topological insulators and superconductors," Rev. Mod. Phys. **83**, 1057–1110 (2011).
3. H. Zhang, S. B. Lu, J. Zhang, J. Du, S. C. Wen, D. Y. Tang, and K. P. Loh, "Molybdenum disulfide (MoS_2) as a broadband saturable absorber for ultra-fast photonics," Opt. Express **22**, 7249–7260 (2014).
4. B. H. Chen, X. Y. Zhang, K. Wu, H. Wang, J. Wang, and J. P. Chen, "Q-switched fiber laser based on transition metal dichalcogenides MoS_2, $MoSe_2$, WS_2, and WSe_2," Opt. Express **23**, 26723–26737 (2015).
5. S. Schön, M. Haiml, and U. Keller, "Ultrabroadband AIGaAs/CaF_2 semiconductor saturable absorber mirrors," Appl. Phys. Lett. **77**, 782–784 (2000).
6. A. Martinez, A. R. Gallian, P. Marine, V. Fedorov, S. Mirov, and V. Badikov, "Fe:ZnSe and ZnS polycrystalline passive Q-switching of 2.8 μm Er:Cr:YSGG laser," in *Proceedings of Advanced Solid-state Photonics (ASSP)* (Optical Society of America, 2007), paper TuB24.
7. S. X. Wang, H. H. Yu, and H. J. Zhang, "Band-gap modulation of two-dimensional saturable absorbers for solid-state lasers," Photon. Res. **3**, A10–A20 (2015).
8. K. F. Mak, M. Y. Sfeir, Y. Wu, C. H. Liu, J. A. Misewich, and T. F. Heinz, "Measurement of the optical conductivity of graphene," Phys. Rev. Lett. **101**, 196405 (2008).
9. M. Z. Hasan and C. L. Kane, "Colloquium: topological insulators," Rev. Mod. Phys. **82**, 3045–3067 (2010).
10. S. X. Wang, H. H. Yu, H. J. Zhang, A. Z. Wang, M. W. Zhao, Y. X. Chen, L. M. Mei, and J. Y. Wang, "Broadband few-layer MoS_2 saturable absorbers," Adv. Mater. **26**, 3538–3544 (2014).
11. V. Tran, R. Soklaski, Y. F. Liang, and L. Yang, "Layer-controlled band gap and anisotropic excitons in few-layer black phosphorus," Phys. Rev. B **89**, 235319 (2014).
12. B. T. Zhang, F. Lou, R. W. Zhao, J. L. He, J. Li, X. C. Su, J. Ning, and K. J. Yang, "Exfoliated layers of black phosphorus as saturable absorber for ultrafast solid-state laser," Opt. Lett. **40**, 3691–3694 (2015).
13. J. Sotor, G. Sobon, W. Macherzynski, P. Paletko, and K. M. Abramski, "Black phosphorus saturable absorber for ultrashort pulse generation," Appl. Phys. Lett. **107**, 051108 (2015).
14. J. Sotor, G. Sobon, M. Kowalczyk, W. Macherzynski, P. Paletko, and K. M. Abramski, "Ultrafast thulium-doped fiber laser mode locked with black phosphorus," Opt. Lett. **40**, 3885–3888 (2015).
15. Z. W. Wang, R. W. Zhao, J. L. He, B. T. Zhang, J. Ning, Y. R. Wang, X. C. Su, J. Hou, F. Lou, K. J. Yang, Y. S. Fan, J. T. Bian, and J. S. Nie, "Multi-layered black phosphorus as saturable absorber for pulsed Cr:ZnSe laser at 2.4 μm," Opt. Express **24**, 1598–1603 (2016).
16. L. C. Kong, Z. P. Qin, G. Q. Xie, Z. N. Guo, H. Zhang, P. Yuan, and L. J. Qian, "Multilayer black phosphorus as broadband saturable absorber for pulsed lasers from 1 to 2.7 μm wavelength," arXiv: 1508.04510 (2015).
17. Z. P. Qin, G. Q. Xie, H. Zhang, C. J. Zhao, P. Yuan, S. C. Wen, and L. J. Qian, "Black phosphorus as saturable absorber for the Q-switched Er:ZBLAN fiber laser at 2.8 μm," Opt. Express **23**, 24713–24718 (2015).
18. Z. P. Qin, G. Q. Xie, C. J. Zhao, S. C. Wen, P. Yuan, and L. J. Qian, "Mid-infrared mode-locked pulse generation with multilayer black phosphorus as saturable absorber," Opt. Lett. **41**, 56–59 (2016).
19. M. Robinson and D. P. Devor, "Thermal switching of laser emission of Er^{3+} at 2.69 μ and Tm^{3+} at 1.86 μ in mixed crystals of CaF_2:ErF_3:TmF_3," Appl. Phys. Lett. **10**, 167–170 (1967).
20. R. C. Stoneman, J. G. Lynn, and L. Esterowitz, "Direct upper-state pumping of the 2.8 μm Er^{3+}:YLF laser," IEEE J. Quantum Electron. **28**, 1041–1045 (1992).
21. C. Kränkel, "Rare-earth-doped sesquioxides for diode-pumped high-power lasers in the 1-, 2-, and 3-μm spectral range," J. Sel. Top. Quantum Electron. **21**, 1602013 (2014).
22. T. Sanamyan, M. Kanskar, Y. Xiao, D. Kedlaya, and M. Dubinskii, "High power diode-pumped 2.7-μm Er^{3+}:Y_2O_3 laser with nearly quantum defect-limited efficiency," Opt. Express **19**, A1082–A1087 (2011).
23. T. Li, K. Beil, C. Kränkel, and G. Huber, "Efficient high-power continuous wave Er:Lu_2O_3 laser at 2.85 μm," Opt. Lett. **37**, 2568–2570 (2012).
24. M. Q. Fan, T. Li, S. Z. Zhao, G. Q. Li, H. Y. Ma, X. C. Gao, C. Kränkel, and G. Huber, "Watt-level passively Q-switched Er:Lu_2O_3 laser at 2.84 μm using MoS_2," Opt. Lett. **41**, 540–543 (2016).
25. M. Skorczakowski, J. Swiderski, W. Pichola, P. Nyga, A. Zajac, M. Maciejewska, L. Galecki, J. Kasprzak, S. Gross, A. Heinrich, and T. Bragagna, "Mid-infrared Q-switched Er:YAG laser for medical applications," Laser Phys. Lett. **7**, 498–504 (2010).
26. K. L. Vodopyanov and V. Chazapis, "Extra-wide tuning range optical parametric generator," Opt. Commun. **135**, 98–102 (1997).
27. T. H. Allik, S. Chandra, D. M. Rines, P. G. Schunemann, J. A. Hutchinson, and R. Utano, "Tunable 7–12 μm optical parametric oscillator using a Cr, Er:YSGG laser to pump CdSe and $ZnGeP_2$ crystals," Opt. Lett. **22**, 597–599 (1997).
28. H. Liu, A. T. Neal, Z. Zhu, Z. Luo, X. F. Xu, D. Tománek, and P. D. Ye, "Phosphorene: an unexplored 2D semiconductor with a high hole mobility," ACS Nano **8**, 4033–4041 (2014).
29. Z. N. Guo, H. Zhang, S. B. Lu, Z. T. Wang, S. Y. Tang, J. D. Shao, Z. B. Sun, H. H. Xie, H. Y. Wang, X. F. Yu, and P. K. Chu, "From black phosphorus to phosphorene: basic solvent exfoliation, evolution of Raman scattering, and applications to ultrafast photonics," Adv. Funct. Mater. **25**, 6996–7002 (2015).
30. S. B. Lu, L. L. Miao, Z. N. Guo, X. Qi, C. J. Zhao, H. Zhang, S. C. Wen, D. Y. Tang, and D. Y. Fan, "Broadband nonlinear optical response in multi-layer black phosphorus: an emerging

infrared and mid-infrared optical material," Opt. Express **23**, 11183–11194 (2015).
31. A. C. Gomez, L. Vicarelli, E. Prada, J. O. Island, K. L. N. Acharya, S. I. Blanter, D. J. Groenendijk, M. Buscema, G. A. Steele, J. V. Alvarez, H. W. Zandbergen, J. J. Palacios, and H. S. J. Zant, "Isolation and characterization of few-layer black phosphorus," 2D Mater. **1**, 025001 (2014).
32. Y. W. Wang, G. H. Huang, H. R. Mu, S. H. Lin, J. Z. Chen, S. Xiao, Q. L. Bao, and J. He, "Ultrafast recovery time and broadband saturable absorption properties of black phosphorus suspension," Appl. Phys. Lett. **107**, 091905 (2015).
33. H. D. Xia, H. P. Li, C. Y. Lan, C. Li, J. B. Du, S. J. Zhang, and Y. Liu, "Few-layer MoS_2 grown by chemical vapor deposition as a passive Q-switcher for tunable erbium-doped fiber lasers," Photon. Res. **3**, A92–A96 (2015).
34. C. Wei, X. S. Zhu, F. Wang, Y. Xu, K. Balakrishnan, F. Song, R. A. Norwood, and N. Peyghambarian, "Graphene Q-switched 2.78 μm Er^{3+}-doped fluoride fiber laser," Opt. Lett. **38**, 3233–3236 (2013).
35. J. F. Li, H. Y. Luo, L. L. Wang, C. J. Zhao, H. Zhang, H. P. Li, and Y. Liu, "3-μm mid-infrared pulse generation using topological insulator as the saturable absorber," Opt. Lett. **40**, 3659–3662 (2015).